An Analytical Model of Induction Motors for Rotor Slot Parametric Design Performance Evaluation

Ahamed Ibrahim Sithy Juhaniya[1], Ahmad Asrul Ibrahim[2], Muhammad Ammirrul Atiqi Mohd Zainuri[3], Mohd Asyraf Zulkifley[4]
Dept. Electrical, Electronic and Systems Engineering, Faculty of Engineering and Built Environment
Universiti Kebangsaan Malaysia, 43600 UKM Bangi, Malaysia

***Abstract*—Induction motors are commonly used in most electricity generation due to their low investment cost. However, the performance of the induction motors for different applications highly depends on rotor design and machine geometry. For example, changing rotor bar height and width varies the rotor resistance and reactance, thereby leading to variation of the motor efficiency. A parametric study on rotor slot geometry parameters such as opening height, rotor slot depth, and rotor slot width, is carried out to investigate the effect of the parameters on the efficiency of a squirrel cage induction motor. The study is based on analytical model that considers a general-purpose squirrel cage induction motor with the specification of 5.5 kW, 60 Hz, and 460 V. The analytical model is developed and simulated within the MATLAB software environment. The effects of each parameter variation toward efficiency of the induction motor are investigated individually as well as all together using a 4D scatter plot. Results show that the efficiency can be improved up to 0.1% after designing a suitable setting of rotor slot parameters from the initial settings.**

***Keywords*—Analytical model; efficiency; induction motor; rotor slot parameters**

I. Introduction

Electrical machine is widely used for electromechanical energy conversion either to operate as generator or motor [1]. The electrical machines can be categorized as motors and generators depending on their energy conversion mechanism. They are considered electrical motors when they convert electrical energy into mechanical energy. Among various types of electrical motors, DC motors, synchronous motors, and induction motors are more popular for applications in residential and industrial [2], [3]. On one hand, DC motors require commutation mechanisms in their operation, leading to high maintenance cost. On the other hand, the synchronous motors are very expensive due to the use of high-cost permanent magnets; furthermore, they require starting mechanisms. Therefore, the induction motor is a promising option for electromechanical energy conversion applications [4] because this type of electrical machines is a low cost, low maintenance, and self-starting mechanism. Although the induction motors are favorable for many applications; they suffer from some disadvantages particularly low efficiency [5]. Efficiency is an important indicator to show the performance of an electrical motor. It can be improved by modeling the electrical motor using optimal parameter settings [6]. Among the design parameters of the electrical motor, rotor slot geometry parameters provide more effect to its performance. This condition is mainly due to the rotor slot design, which determines the resistance and leakage reactance of the electrical motor.

Several works have been carried out in the past few years to improve the performance of induction motors by redesigning the rotor slot. In [2], various shapes of rotor bar were considered to determine the best shape that provides the highest efficiency with minimum overall cost. The effect of using different materials specifically aluminium and copper for the rotor bar were studied in [7]. Flux2D software was used in [8] to carry out a parametric study of rotor slot design using a finite element method (FEM) technique to showcase their effect on the behavior of induction motors, such as flux distribution and power losses. The FEM technique was also used in [9] to study the impact of changing rotor slot parameters toward the induction motor performance, total harmonic distortion and starting characteristics of the motor. In [10], the FEM technique was used to analyze the electromagnetic characteristics of induction motors using various shapes of rotor bars to obtain the best design. Apart from studying normal rotor bar shapes, the effect of broken rotor bar and different stator slot opening settings were tested using FEM technique to evaluate the induction motor performance [6], [11]. Investigation on the rotor bar shapes was also carried out in [12], but they focused on generator rather than motor applications.

In the previous works, the investigation of changing the rotor slot geometry parameters was mainly based on 2D analysis instead of 3D analysis, which provides less accurate results. The FEM technique, which is based on a commercial software, is not flexible because of computational burden particularly for the parametric study at the initial design process. Furthermore, the important performance parameters, such as efficiency, could not be appropriately addressed. Therefore, this work is carried out to investigate the effect of changing rotor slot parameters toward efficiency of the induction motor using an analytical model. In the following section, the basic principles of induction motor is discussed to provide better understanding before the analytical model to calculate efficiency can be constructed. Then, a development of the analytical model is explained in Section III. In Section IV, results on varying rotor slot parameters are showcased and discussed. Finally, a conclusion of the research work is drawn in Section V.

II. Efficiency of Induction Motor

Induction motors are used in most applications to fulfill either industrial and domestic needs known as workhorse of modern industry [13]. The induction motor can be divided into two types: 1) wound rotor induction motor and 2) squirrel cage induction motors. The squirrel cage type is widely used in the

industrial applications because of its idiosyncratic characteristics, such as simplicity, robustness, easy maintenance, and low cost [14]. Therefore, a squirrel cage induction motor model is used in this work.

Operational principles of squirrel cage induction motor are very much similar to transformers. Two magnetic circuits in transformers, referred to as primary and secondary windings, are isolated by a small air-gap. The circuits can be represented as two relatively movable windings which are called stator and rotor in the induction motor [14], [15]. The stator winding of the three-phase squirrel cage induction motor is connected to the three-phase AC source either in a star or delta configuration. Current is supplied to the rotor circuit by the process of electromagnetic induction [16] from the magnetic field of stator circuit. The induction motor is called a singly excited machine because the rotor has no external source. The induction motors are considered self-starting motors because they do not require any external means during the starting condition [17]. Induction motor normally operates at a speed that slightly lower than its synchronous speed; therefore, it is known as asynchronous motor. The difference between operating speed and synchronous speed is known as slip speed of the motor.

Understanding the power losses of the induction motor is important before its efficiency can be calculated. Power flow diagram, as shown in Fig. 1, is used to illustrate the power losses of induction motor. Power transfer from stator to rotor is referred as the airgap power loss, P_{ag}. P_{ag} is calculated by taking into account stator copper losses, P_{sc} and iron losses, P_{iron} as expressed in (1). On the other hand, the conversion power loss, P_{conv} is the total electrical output power from the rotor after subtraction of all types of electrical losses. P_{conv} is calculated by subtracting the rotor copper losses from the airgap power loss. Rotor copper losses, P_{rc} are copper losses generated inside the rotor due to the rotor internal resistance. The output power of the motor is obtained by considering all the losses due to the rotational motion of the rotor shaft. The losses related with rotation motion of the shaft consist of mechanical and ventilation power losses, P_{mv} and stray power losses, P_{stray}.

$$P_{ag} = P_{input} - P_{sc} - P_{iron} \tag{1}$$

$$P_{conv} = P_{ag} - P_{rc} \tag{2}$$

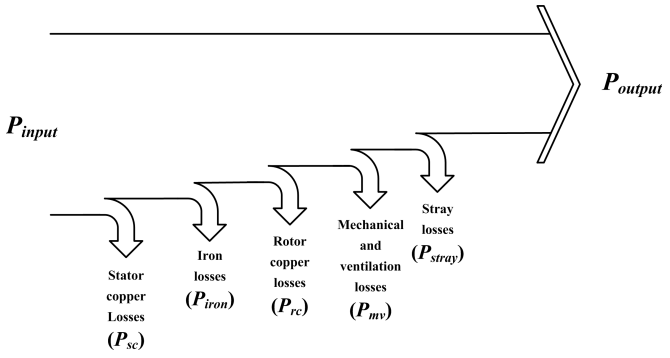

Fig. 1. Power flow diagram of induction motor [15], [16], [17]

Total power loss of induction motor can be calculated as follows:

$$P_{loss} = P_{sc} + P_{rc} + P_{iron} + P_{stray} + P_{mv} \tag{3}$$

The value of P_{mv} can be obtained depending on the number of poles, as shown in Table I. In this work, a four-pole induction motor is considered; therefore, the mechanical and ventilation losses are 1.2% of the output power.

TABLE I. MECHANICAL AND VENTILATION LOSSES, P_{mv} [18]

No. of poles	P_{mv}
2	$0.03 \times P_{out}$
4	$0.012 \times P_{out}$
6,8	$0.08 \times P_{out}$

The stator copper losses, P_{sc} due to resistance in the stator winding can be calculated using stator current, I_s and stator resistance, R_1 as expressed in (4). On the contrary, the rotor copper losses, P_{rc} due to resistance in the rotor winding can be obtained from the rotor current, I_r and rotor resistance, R_2 using expression in (5). The values of R_1 and R_2 can be derived from stator and rotor slot modeling subsections that will be discussed in detail subsequently in the induction motor modeling section.

$$P_{sc} = 3(I_s)^2 R_1 \tag{4}$$

$$P_{rc} = 3(I_r)^2 R_2 \tag{5}$$

The iron losses, P_{iron} are the summation of stator tooth iron losses, P_{st}, stator yoke iron losses, P_{sy}, and tooth flux pulsation core losses, P_{tp}, as follows:

$$P_{iron} = P_{st} + P_{sy} + P_{tp} \tag{6}$$

The stator tooth iron losses, P_{st} can be calculated as follows:

$$P_{st} = K_T P'(f/50)^{1.3} B_{TS}^{1.7} W_T \tag{7}$$

where f refers to frequency, K_T represents the core loss augmentation due to mechanical machining, and P' is the specific weight losses in W/kg at 1.0 T and 50 Hz. The value of P' is normally between 2 and 3 W/kg as used by the manufacturer [11]. B_{TS} is the stator tooth flux density, and W_T is the weight of the stator tooth. In this model, B_{TS} and W_T are set to 1.55 T and 4 kg, respectively.

The stator yoke iron losses, P_{sy} can be determined using the following formula:

$$P_{sy} = K_Y P'(f/50)^{1.3} B_C^{1.7} W_Y \tag{8}$$

where K_Y stands for the mechanical machining factor of the stator yoke that normally takes the value in the range between 1.6 and 1.9. B_C and W_Y represent yoke flux density of stator and weight of the stator, respectively.

The tooth pulsation core losses, P_{tp} are neglected because the value is remarkably smaller than the iron losses related with stator tooth and stator yoke.

The stray losses, P_{stray} include the core losses associated with rotor surface and space harmonic cage losses. In most

applications, the stray losses are considered by the manufacturers as 1% of the expected output power of the motor [19] and can be expressed as follows:

$$P_{stray} = 0.01 \times P_{out} \tag{9}$$

The efficiency of induction motor, η can be obtained from the total power losses, P_{loss} and output power, P_{out} using the following expression:

$$\eta = \frac{P_{out}}{(P_{out} + P_{loss})} \tag{10}$$

III. Modeling of Induction Motor

Fig. 2 shows an equivalent circuit of the induction motor as referred to the stator side using the concept of transformer modeling. The stator winding resistance, R_1 represents copper losses in the stator, and the stator winding reactance, X_1 represents leakage flux of the stator. The magnetization reactance, X_m represents magnetization effect of the induction motor. R_2 and X_2 are rotor resistance and rotor leakage reactance, respectively.

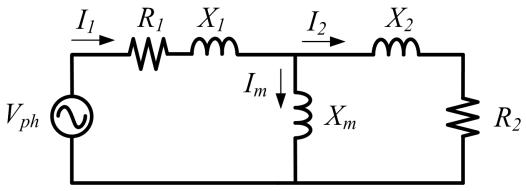

Fig. 2. Equivalent circuit of induction motor

An induction motor can be modelled using equations derived from the per phase equivalent circuit in Fig. 2. In this work, a 5.5 kW, 460 V, and 60 Hz squirrel cage induction motor is considered; its specifications are tabulated in Table II. Single-cage type slots are used for rotor and stator slots.

TABLE II. Motor Specifications

Parameters	Values
Output power(kW)	5.5
Frequency(Hz)	60
Rated voltage (V)	460
Power factor	0.83
No. phase	3
No. poles	4

Fig. 3 shows a quarter section of an induction motor model where all the parameters should be obtained to fulfill the design requirement. Parameter settings of the induction motor are presented in Table III. The parameter stack length refers to the total length of lamination stack, which provides rigidity to the stator. Stack length excludes the end ring length.

A. Stator Slot Design

Fig. 4 illustrates a shape of stator slot and its geometry parameters that can be used to calculate the stator resistance (R_1) and stator leakage reactance (X_1). This work provides focus on the rotor slot parameters; thus, all stator slot dimensions

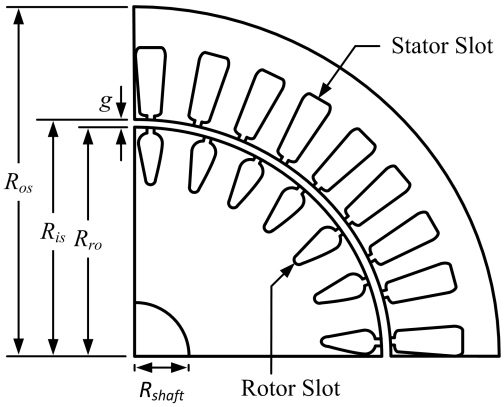

Fig. 3. Quarter section of an induction motor

TABLE III. Induction Motor Parameter Settings

Parameters	Dimension
Stator outer radius (R_{os})	90 mm
Stator inner radius (R_{is})	56 mm
Rotor outer radius (R_{ro})	55.65 mm
Rotor shaft radius (R_{shaft})	17.5 mm
Airgap length (g)	0.35 mm
Stack length	132 mm
No. stator slots (N_s)	36
No. rotor slots (N_r)	28

are fixed as shown in Table IV. R_1 and X_1 can be calculated using the following expressions:

$$R_1 = \frac{L_c W}{A_{co} a_1} \times R_{co} \tag{11}$$

$$X_1 = \frac{2\mu_o \omega L_c W^2}{pq(\lambda_s + \lambda_{ds} + \lambda_{es})} \tag{12}$$

where L_c is the stator coil length, W is the number of turns in stator windings, A_{co} is the area of a conductor, a_1 is the number of parallel current paths, R_{co} is the resistivity of the copper, p is the number of poles, and q is the number of stator slot per pole per phase; λ_s, λ_{ds} and λ_{es} are the stator slot, differential and end ring coefficients, respectively.

The stator slot coefficient (λ_s) can be calculated as follow:

$$\lambda_s = \left[\frac{2H_s}{3\,(B_{s1} + B_{s2})} + \frac{2H_w}{(B_{os} + B_{s1})} + \frac{H_{os}}{B_{os}}\right] \times \left(\frac{1 + 3\beta}{4}\right) \tag{13}$$

β is known as chording factor, which takes the values in range as follows:

$$\frac{2}{3} \leq \beta \leq 1 \tag{14}$$

The stator differential coefficient (λ_{ds}) is calculated using

the following expression:

$$\lambda_{ds} = \frac{0.9\tau_s q^2 {K_w}^2 (0.18\sin\phi + 1.24)}{1.21g(1+K_{st})} \times \left[1 - 0.033\ \frac{{B_{os}}^2}{g\tau_s}\right] \quad (15)$$

$$\phi = \pi(6\beta - 5.5) \quad (16)$$

where τ_s is the slot pitch of the stator, K_w accounts for winding factor, and K_{st} is the saturation factor. The stator end ring coefficient (λ_{es}) can be obtained from the following:

$$\lambda_{es} = 0.34\ \frac{q}{L}(L_{es} - 0.64\ \beta\tau) \quad (17)$$

where L is the stack length, L_{es} is the stator end ring length, and τ is the pole pitch. R_1 and X_1 are calculated using the values given in the Table IV, and they take the values 0.94 and 2.16 Ω, respectively.

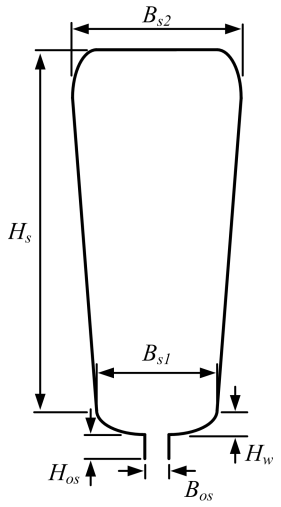

Fig. 4. Design of stator slot

TABLE IV. STATOR SLOT PARAMETER SETTINGS

Parameters	Length(mm)
B_{os}	2.5
B_{s1}	5.4
B_{s2}	9.2
H_{os}	2
H_w	1.5
H_s	20.4

B. Rotor Slot Design

The geometry parameters for rotor bar design are shown in Fig. 5. Resistance and reactance of the rotor can be derived from the rotor bar design parameters. The rotor bar design parameters are rotor slot opening height (Hor), rotor slot height (Hr), rotor slot tooth width (Btr), rotor slot opening width (Bor), rotor slot lower width (B_{r1}), and rotor slot upper width (B_{r2}). In this study, Bor is fixed to a constant value at 1.5 mm because the number of rotor slot remains the same throughout the work, causing constant magnetization effect [11]. In addition, B_{r1} and B_{r2} depend on the Hor, Hr and Btr as expressed in (18) and (19).

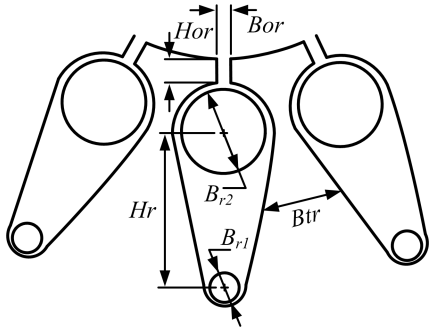

Fig. 5. Design of rotor slot

$$B_{r1} = \frac{\pi(Bor - 2Hor) - N_r Btr}{\pi + N_r} \quad (18)$$

$$B_{r2} = B_{r1} + 2Hr\tan(\frac{\pi}{N_r}) \quad (19)$$

Then, rotor resistance (R_2) and rotor leakage reactance (X_2) can be calculated using the following expressions:

$$R_2 = \frac{4m(WK_w)^2 R_{co}}{N_r}\left[\frac{LK_R}{A_b} + \frac{L_{er}}{2A_{er}\sin(\frac{\pi p}{N_r})^2}\right] \quad (20)$$

$$X_2 = \frac{4m(WK_w)^2\omega\mu_o L}{N_r(\lambda_r K_x + \lambda_{dr} + \lambda_{er})} \quad (21)$$

where m is the number of phases, K_w is the winding factor, K_R is skin effect coefficient for resistance, A_b is the area of rotor slot, L_{er} is the rotor end ring length, A_{er} is the area of rotor end ring, and K_x is the skin effect coefficient for rotor reactance. λ_r, λ_{dr} and λ_{er} are the permeance values of the rotor slot, differential and end ring coefficients, respectively.

The end ring and skin effects on the resistance and reactance of the rotor are also considered in the rotor resistance and reactance calculation. Equation (20) represents total resistance of the rotor including end ring part resistance and resistance due to the rotor slot [20].

IV. RESULTS AND DISCUSSION

This work focuses on the design of rotor slot, where Bor is fixed. Table V shows the dimension constraints of rotor slot to ensure that it does not violate the considered size of the induction motor as given in Table III. As a reference, the initial values of Hor, Btr and Hr are set to 0.5 mm, 4.25 mm and 14 mm, respectively the same as that in [11]. Fig. 6 depicts the variation of efficiency over increasing motor speed. It clearly shows that the motor synchronous speed is 1800 rpm at 60 Hz frequency. On the contrary, the efficiency at the rated speed (1757 rpm) is observed at 89.7%. The effect of changing the rotor slot parameters (Hor, Hr and Btr) on motor efficiency will be discussed in detail in the following subsections:

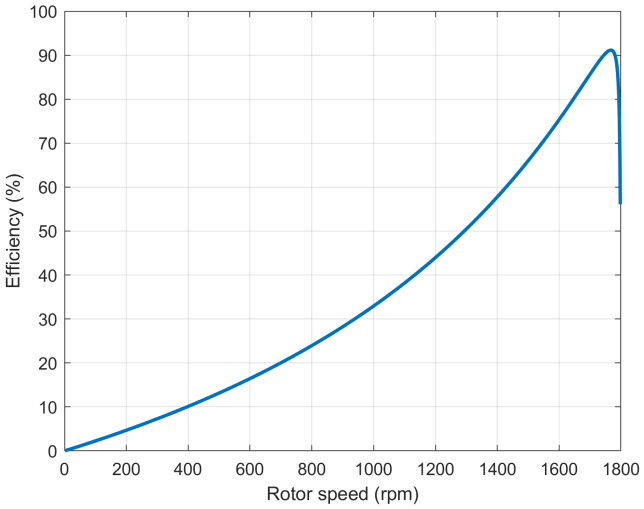

Fig. 6. Performance of the induction motor at initial settings

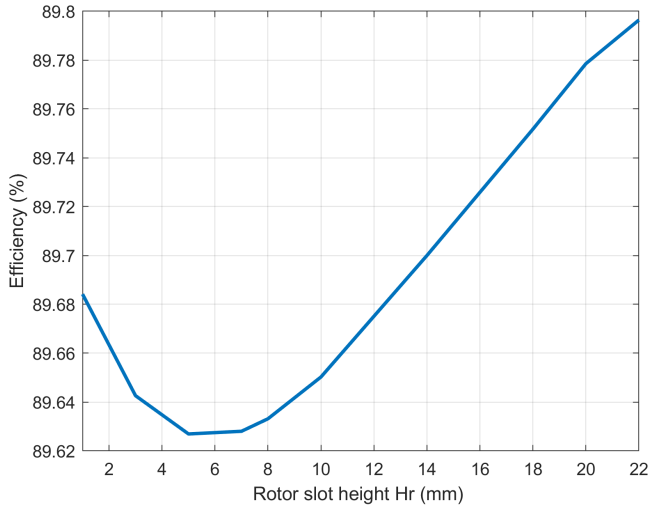

Fig. 7. Individual variation of efficiency when changing Hr

TABLE V. ROTOR SLOT GEOMETRY PARAMETER SETTINGS

Parameters	Length(mm)	
	Min	Max
Hor	0.5	5
Btr	2	5.5
Hr	1	22

A. Effect of Changing Rotor Slot Height

In this case study, the rotor slot height, Hr is varying within the limits as given in Table V, whereas the other parameters are maintained in the initial condition. Fig. 7 shows the variations of efficiency when changing Hr between 1 and 22 mm. Evidently, the efficiency increases with increasing Hr value from the initial point at 14 mm. A significant improvement in the effective area of the rotor slot can be obtained at higher value of Hr which reduces the rotor resistance. Copper losses related to the rotor slot also decreased due to the lower resistance, resulting in higher efficiency. When reducing Hr below 14 mm, the efficiency decreases up to 89.63% at $Hr = 5$ mm, and then rebounds. In this case, the effect of increasing the rotor resistance continues when decreasing Hr. However, the lower value of Hr causes the depth of the rotor slot to reduce, leading to the flux lines coupled with the stator lines. As a result, the leakage reactance of the rotor is reduced; therefore, the efficiency is improved. At a certain point, the leakage reactance becomes more dominant than the effect of increment on the rotor resistance (might be due to less effect on the effective area of the rotor slot). As can be seen from the figure, the highest value of efficiency (89.79%) can be obtained when Hr is at the upper bound, at 22 mm. At this setting, the efficiency can be improved by 0.09% as compared with the initial condition.

B. Effect of Changing Rotor Slot Opening Height

Fig. 8 shows the variations of efficiency when the rotor slot opening height, Hor varies between 0.5 and 5 mm. In this case study, Hr and Btr are maintained at the initial condition at 14 and 4.25 mm, respectively. As shown in the figure, efficiency slightly decreases until $Hor = 2.5$ mm, and then, it steeply increases to the highest value at 89.715% when $Hor = 5$ mm. The efficiency can be improved up to 0.015% compared with the initial condition for individual Hor settings. It is important to notice that Hor provides less impact on the efficiency than Hr. This finding is mainly because the Hor is located very close to the stator surface area in which the flux lines through the Hor are almost coupled with the stator flux lines. Therefore, significant improvement in efficiency is difficult to obtain when changing Hor.

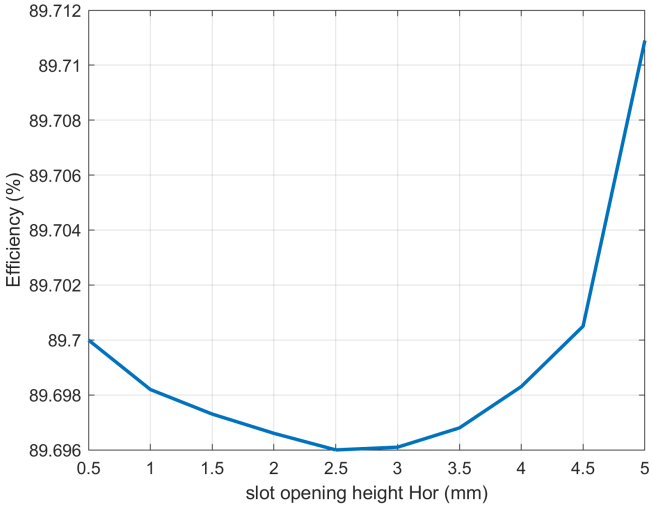

Fig. 8. Individual variation of efficiency when changing Hor

C. Effect of Changing Rotor Slot Tooth Width

Fig. 9 depicts the variation of efficiency when varying the rotor slot tooth width, Btr. In this case study, Btr is varied between 2 and 5.5 mm, whereas Hr and Hor are maintained

at the initial condition at 14 and 0.5 mm, respectively. The range of Btr is based on the number of rotor slot in Table III. The figure shows that variations of efficiency have completely different pattern from the previous results, where the efficiency drastically drops in the middle because reactance and resistance become dominant at this value. The highest efficiency at 89.78% can be achieved when Btr is set to 3.75 mm. The efficiency can be improved by 0.08% as compared with the initial condition.

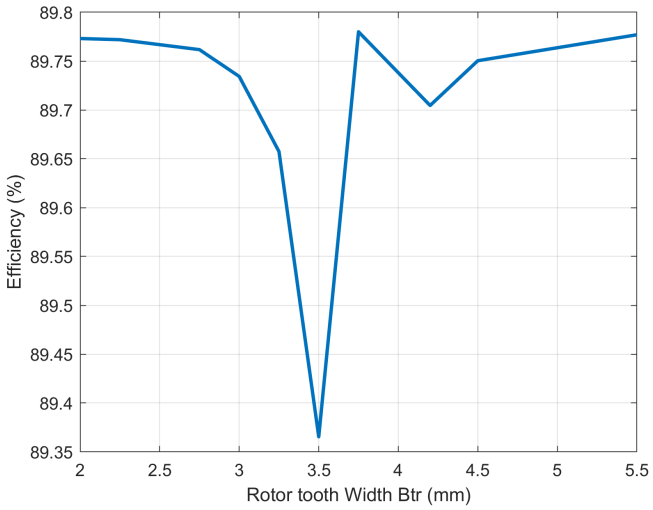

Fig. 9. Individual variation of efficiency when changing Btr

D. Effect of Changing All Selected Parameters

In previous subsections, the effect of individual parameters on efficiency have been discussed, but they could not explain the overall effect of changing Hr, Hor, and Btr simultaneously. Therefore, a 4D plot is used in this subsection to explain the effect of changing all selected rotor slot parameters. Fig. 10 shows a 4D scatter plot of efficiency when changing all the three parameters. The figure shows that the efficiency reaches maximum value at 89.8% when Hr, Hor and Btr at the maximum settings or more specifically at 22, 5, and 5-5.5 mm, respectively as highlighted by red circle. When all parameters are at maximum settings, the overall area covered by the rotor slot is increased and leads to a significant reduction in rotor resistance. Therefore, copper losses can be reduced, and the efficiency is improved. Among the three parameters, Hr provides the highest influence to the efficiency improvement, followed by Btr as shown by arrows in the figure.

V. Conclusion

This paper presents an analytical approach to investigate the influence of rotor slot geometry parameters on motor efficiency. An analytical model of three-phase squirrel cage induction motor was developed within a MATLAB environment for the investigation purposes. Several case studies were carried out and they can be categorized into individual and amalgamated changing of rotor slot parameters. In the individual case studies, the effects of changing each individual rotor slot geometry parameters namely, rotor slot height (Hr), rotor

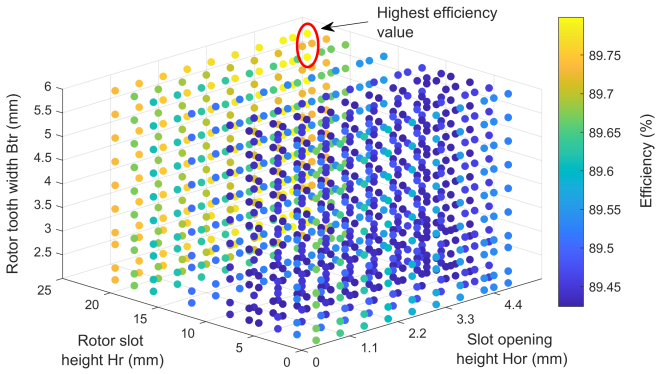

Fig. 10. 4D Scatter Plot of Efficiency when Changing All Parameters

slot opening height (Hor) and rotor slot tooth width (Btr) were analyzed. The results show that the maximum efficiency can be obtained up to 89.79%, 89.715%, and 89.78% (0.09%, 0.015%, and 0.08% improvement from the initial condition) when changing the individual parameter of Hr, Hor and Btr, respectively. However, the results cannot sufficiently explain how much the improvement can be achieved when considering all parameters. Therefore, the three parameters were changed and analyzed together in the amalgamated case study. In this case, the efficiency can be increased up to 0.1% compared with the initial condition or achieve the maximum value at 89.8%. It clearly shows that the performance of a squirrel cage induction motor can be improved substantially when the selected rotor slot geometry parameters are set appropriately. However, this approach is limited to only three parameters as presented in this paper. Thus, an optimization approach can be used in the future to solve the problem when considering more parameters.

Acknowledgment

The authors would like to thank Universiti Kebangsaan Malaysia for funding the research under grant GGPM-2019-031.

References

[1] A. Boglietti, A.M. Elrefaie, O. Drubel, A.M. Omekanda, N. Bianchi, E.B. Agamloh, M. Popescu, A.D. Gerlando and J.B. Bartolo. “Electrical machine topologies: Hottest topics in the electrical machine research community,” IEEE Industrial Electronics Magazine, vol. 8, no. 2, pp. 18-30, 2014.

[2] Q. Ding, Z. Yang, X. Sun, Q. Zhao and H. Zhu. “Analysis of rotor slot width influence on a bearingless induction motor,” Computers and Electrical Engineering, vol. 81, pp. 1-16, 2019.

[3] M. Sellami and S. Tounsi. “Control of axial flux DC motor with permanent magnet dedicated to electric traction,” International Journal of Electrical Components and Energy Conversion, vol. 1, no. 1, pp. 44-48, 2015.

[4] R.J. Swaraj and T. Archana. “Comparison of electric motors for electric vehicle applications,” International Journal of Research in Engineering and Technology, vol. 6, no. 9, pp. 12-17, 2017.

[5] W. Zhikun, C.T.Z.E. Wood, H. Shaojia, W. Hongtao and X. Tao. “Challenges faced by electric vehicle motors and their solutions,” IEEE Access, vol. 9, pp. 5228-5249, 2020.

[6] E. Makhetha, M. Muteba and D.V. Nicolae. "Effect of rotor bar shape and stator slot opening on the performance of three phase squirrel cage induction motors with broken rotor bars," Southern African Universities Power Engineering Conference/Robotics and Mechatronics/Pattern Recognition Association of South Africa, 2019, pp. 463-468.

[7] K.A.I. Daut, K. Anayet, N. Gomesh, M. Asri and Y.M. Irwan. "Comparison of copper rotor bars with aluminium rotor bars using FEM software: A performance evaluation," International Conference on Computer and Electrical Engineering, 2009, pp. 453-456.

[8] V.A. Galindo, X.M. Lopez-Fedez, J.A.D. Pinto and A.P. Coimbra. "Parametric study of rotor slot shape on a cage induction motor," International Symposium on Electromagnetic Fields in Electrical Engineering, 2002, pp. 190-195.

[9] K.N. Gyftakis and J. Kappatou. "The impact of the rotor slot number on the behaviour of the induction motor," Advances in Power Electronics, pp. 837010, 2013.

[10] J. Kappatou, K. Gyftakis and A. Safacas "FEM study of the rotor slot design influences on the induction machine characteristics," Advanced Computer Techniques in Applied Electromagnetics, vol. 30, pp. 247-252, 2007.

[11] E. Maloma, M. Muteba and D. Nicolae. "Effect of rotor bar shape on the performance of three phase induction motors with broken rotor bars," International Conference on Optimization of Electrical and Electronic Equipment, 2017, pp. 364-369.

[12] A. Leicht and K. Makowski. "Influence of shape and material of rotor bars on performance characteristics of single-phase self-excited induction generators," International Journal for Computation and Mathematics in Electrical and Electronic Engineering, vol. 38, no. 4, pp. 1235-1244, 2019.

[13] I. Daut, K. Anayet and A. Fauzi. "Development of copper rotor of AC induction motor," Australian Journal of Basic and Applied Sciences, vol. 4, no. 12, pp. 5941-5946, 2010.

[14] J. Singh, K. Singh and H. Kaur. "Designing of three phase squirrel cage induction motor for good efficiency," International Journal of Engineering and Innovative Technology, vol. 5, no. 7, pp. 40-45, 2016.

[15] A.G. Yetgin, M. Turan, B. Cevher, A.İ. Çanakoğlu and A. Gün. "Squirrel cage induction motor design and the effect of specific magnetic and electrical loading coefficient," International Journal of Applied Mathematics Electronics and Computers, vol. 7, no. 1, pp. 1-8, 2019.

[16] J.M. Apsley, S. Williamson, A.C. Smith and M. Barnes. "Induction motor performance as a function of phase number," IEE Proceedings: Electric Power Applications, vol. 153, no. 6, pp. 898-904, 2006.

[17] M.A. Iqbal and V. Agarwal. "Investigation & analysis of three phase induction motor using finite element method for power quality improvement," International Journal of Electronic and Electrical Engineering, vol. 7, no. 9, pp. 901-908, 2014.

[18] I. Boldea and S.A. Nasar. "The induction machines design handbook," Taylor and Francis Group, 2010.

[19] D.J. Kim, J.H. Choi, Y.D. Chun, D.H. Koo and P.W. Han. "The study of the stray load loss and mechanical loss of three phase induction motor considering experimental results," Journal of Electrical Engineering and Technology, vol. 9, no. 1, pp. 121-126, 2014.

[20] A. Boglietti, A. Cavagnino and M. Lazzari. "Geometrical approach to induction motor design," The 33rd Annual Conference of the IEEE Industrial Electronics Society, 2007, pp. 149-156.